ELSEVIER

Journal of Atmospheric and Solar-Terrestrial Physics 67 (2005) 219–228

Journal of ATMOSPHERIC AND SOLAR-TERRESTRIAL PHYSICS

www.elsevier.com/locate/jastp

Observation of the gravity waves from GPS/MET radio occultation data

Y.A. Liou[a,*], A.G. Pavelyev[b], J. Wickert[c]

[a]*Center for Space and Remote Sensing Research, National Central University, Chung-Li, 320, Taiwan, ROC*
[b]*Institute of Radio Engineering and Electronics of the Russian Academy of Sciences, (IRE RAS), Fryazino, Vvedenskogo sq. 1, 141191 Moscow region, Russia*
[c]*GeoForschungsZentrum Potsdam (GFZ-Potsdam), Telegrafenberg, 14473 Potsdam, Germany*

Received 3 May 2003; received in revised form 23 April 2004; accepted 9 August 2004

Abstract

We show that the amplitude of the Global Positioning System (GPS) signals in the radio occultation (RO) experiments is sensitive to the atmospheric wave structures. Earlier the phase of the GPS occultation signals have been used for statistical investigation of the gravity waves (GW) activity in the height interval 10–40 km on a global scale. Analysis of the RO amplitude data revealed wave clusters (quasi-regular structures) with the vertical size of about 10 km and interior vertical period ~0.8–2 km in the tropopause and lower stratosphere. The amplitude RO data may be utilized to determine the temperature vertical profiles and its vertical gradient in the upper troposphere and stratosphere. In the considered RO events variations of the vertical temperature gradient dT(h)/dh corresponding to the amplitude clusters are in the range from −9 K/km to 6 K/km with vertical scales ~1–3 km. We show that these variations can be linked to the GW propagation in the atmosphere. We use the polarization and dispersion relationships and Hilbert transform to find the 1-D GW image in the atmosphere by analyzing the vertical temperature gradient $dT(h)/dh$. The GW image consists of the phase and amplitude of the GW as functions of height. The GW amplitude is non-uniformly distributed with main contribution associated with the tropopause and the secondary maximums in height interval 18–35 km. Using our method we find vertical profiles of the horizontal wind perturbations and their vertical gradient associated with the GW influence. The horizontal wind perturbations are changing in the interval v~2–12 m/s with vertical gradients dv/dh~4–25 m s^{-1} km^{-1}) in the tropopause area and v~ 3–9 m/s, dv/dh ~ 2–15 m/(s km) in the stratosphere for the considered events. For one RO event we compared the estimated values of the horizontal wind perturbations with aero-logical data and found fairly good agreement. The height dependence of the GW vertical wavelength was inferred through the differentiation of the GW phase. Analysis of this dependence using the dispersion relationship for the GW gives estimation of the GW intrinsic phase speed. For the considered events the magnitude of the intrinsic phase speed changes between 1.5–15 m/s at heights 10–40 km. We conclude that the amplitude of the GPS occultation signals contain important information about the GW propagation in the atmosphere on a global scale.

Keywords: GPS radio occultation; Gravity wave; Atmosphere; Amplitude method; Hilbert transform

*Corresponding author. Tel.: +886 3 422 7151; fax: +886 3 425 4908.
E-mail addresses: yueian@csrsr.ncu.edu.tw (Y.A. Liou), pvlv@ms.ire.rssi.ru (A.G. Pavelyev), wickert@gfz-potsdam.de (J. Wickert).

1364-6826/$ - see front matter © 2004 Elsevier Ltd. All rights reserved.
doi:10.1016/j.jastp.2004.08.001

1. Introduction

The gravity waves (GW) in the atmosphere have been observed and modeled for many years (Nagpal, 1979). The GW with horizontal wavelengths ~100–1000 km, vertical wavelengths ~1–10 km, and periods ~10 min–1 h are mainly produced owing to the weather activities (fronts, cyclones, cumulonimbus convection, thunderstorms) and wind flows over irregular topography (mountain waves), and play a decisive role in transporting energy and momentum, in contributing turbulence and mixing, and in affecting the atmospheric circulation and temperature regime (Fritts and Alexander, 2003). Dynamical simulation studies of the stratosphere and mesosphere require a broad spectrum of knowledge including the GW's effects in the empirical models or analytic formulations for a realistic description of the climate changes and variations in the atmospheric, stratospheric and mesospheric global-scale flows (Preusse et al., 1996). Radiosonde (RS) and rocketsonde GW's measurements, balloon soundings, radar observations and lidar studies have been limited to ground-based sites (Eckermann et al., 1995; Sica and Russell, 1999; Nastrom et al., 1997, 2000) mainly over specific land parts of the Northern Hemisphere. Recently a few high-resolution stratospheric satellite instruments have been used to detect GW (Eckermann and Preusse, 1999). However, the time for observations has been limited. This raises the problem of insufficient data for establishing wave climatology for a global scale, despite the good results from many of the ground-based and space-borne instruments (Steiner and Kirchengast, 2000).

Radically new technology incorporates the high-precision radio signals of the Global Positioning System (GPS) at two frequencies $F1 = 1575.42$ and 1227.6 MHz for the GW investigation. The small satellites (e.g., MicroLab-1, installed into a near polar circular orbit with altitude ~750 km) carried a laptop sized GPS receiver to perform remote sensing of the atmosphere and ionosphere by the limb sounding method (Ware et al.,1996; Feng and Herman, 1999). The advantages of the space-borne observations of the atmosphere by the GPS radio signals are that the radio occultation RO technique can recover atmospheric profiles above oceans as well as above land with high vertical resolution (<0.4 km) and accuracy (<1 K in temperature within the upper troposphere and lower stratosphere) (Anthes et al., 2000). Nowadays, new satellite missions CHAMP and SAC-C have been launched to establish global control on the meteorological processes in the atmosphere and phenomena in the ionosphere (Wickert et al., 2001; Reigber et al., 2002; Hajj et al., 2002).

Analysis of the temperature variations found from the RO phase data furnishes an opportunity to investigate the global morphology of the GW activity in the stratosphere and to measure the GW statistical characteristics in the atmosphere as shown by Tsuda et al. (2000), Steiner and Kirchengast (2000), and Tsuda and Hocke (2002). However, these papers were concerned mainly with the GW statistical parameters. The amplitude channels of the RO signal offer new potential and capability for the RO research and for the observation of the quasi-regular structures in the atmospheric and ionospheric waves (Kalashnikov et al., 1986; Pavelyev et al., 2002; Sokolovskiy, 2000; Igarashi et al., 2000, 2001; Liou et al., 2002). Liou et al. (2003) introduced a new analytical method to express the amplitude and phase of the GW as functions of height in the troposphere and stratosphere using the wave trains in the amplitude of the RO signals. They connected the amplitude and phase of the wave trains in the RO amplitude data with the amplitude and phase of the GW using the polarization and dispersion equations for the GW and Hilbert transform. This method opens new perspectives for the GW investigation in the atmosphere and mesosphere using the RO data and as a consequence its capabilities and limitations should be analyzed in detail. The aims of this paper are to describe the connections between the RO amplitude variations and the amplitude and phase of the GW, and to demonstrate the possibility of direct observation of the quasi-regular GW in the atmosphere using the amplitude of the RO signals.

2. Amplitude clusters in ro data

The scheme of the RO experiment is shown in Fig. 1. The point O is the center of the spherical symmetry of the atmosphere. The radio waves emitted by the GPS satellite (point G) are propagating to the receiver onboard of the LEO satellite (point L) along the ray GTL, where T is the tangent point in the atmosphere. The projection of the point T on the Earth's surface determines the co-ordinates of the RO region: latitude φ and longitude λ_l. The vicinity of the point T introduces the major contribution to the changes of the RO signal. Record of the RO signal along the LEO trajectory contains the amplitudes $A1(t)$, $A2(t)$ and phases of the radio field at frequencies $F1$, $F2$ as functions of time.

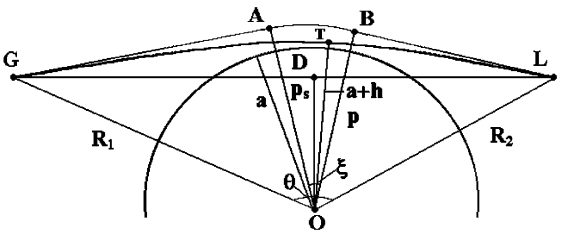

Fig. 1. Key physical and geometric parameters of the RO measurements.

The time interval for the RO measurements τ depends on the orientation between the vertical direction at the point T and the occultation beam path. The time τ is minimal ~30 s, when the orbital planes of the LEO and GPS satellites are parallel. Thus the RO experiments record practically simultaneously the impact of the GW on the RO signal because the GW frequencies are usually well below $1/\tau$, i.e. $0.03\,s^{-1}$. Record of the RO signal $E(t)$ along the LEO trajectory is the radio hologram's envelope that contains the amplitude $A(t)$ and phase $\psi(t) = kS_e(t)$ (k is the wave number in the free space, $S_e(t)$ is the eikonal corresponding to the ray GTL) of the radio field as functions of time:

$$E(t) = A(t)\exp[-i\psi(t)]. \quad (1)$$

Usually only temporal dependence of the phase path excess $S_e(t) - S_s(t)$ is used for retrieving the vertical profiles of the refraction index, temperature in the atmosphere and electron density in the ionosphere, where $S_s(t)$ is the path GTL corresponding to the free space propagation. This is apparently a cause why the measurements of the vertical gradients in the atmosphere and lower ionosphere have been excluded from the attention of the most RO work except for few publications (Vorob'ev et al., 1999, Sokolovskiy, 2000; Igarashi et al., 2000, 2001; Liou et al., 2002). Analysis of the amplitude of the RO signal can give important information for the detection and observation of the wave processes in the atmosphere (Liou et al., 2002; Pavelyev et al., 2002).

Examples of the amplitude variations in the upper troposphere and lower stratosphere are shown in Fig. 2 for sixth RO experiments provided on July 09 and 10, 1995. Wave structures are seen both at the first and second frequencies of GPS signals (amplitudes $A1$ and $A2$ in Fig. 2). Variations of the amplitudes $A1$ and $A2$ are highly correlated. This is a consequence of simultaneous measurements, weak diffraction effects and small values of systematic errors in the amplitude data. These variations give a direct evidence for existing wave structures in the atmosphere. The amplitude variations can give direct information on the form and spatial frequencies associated with the wave structures in the atmosphere. In essence, the quasi-regular amplitude variations represent a radio holographic image of wave processes in the upper troposphere and lower stratosphere. Analysis of the radio holographic amplitude image of the atmosphere can be produced by using the inversion theory developed earlier (Kalashnikov et al., 1986). According to this theory, the amplitude channel of the radio hologram can be used separately from the phase channel to obtain information on the vertical distribution of the refractivity, temperature, and its vertical gradient (Liou et al., 2002). Additional

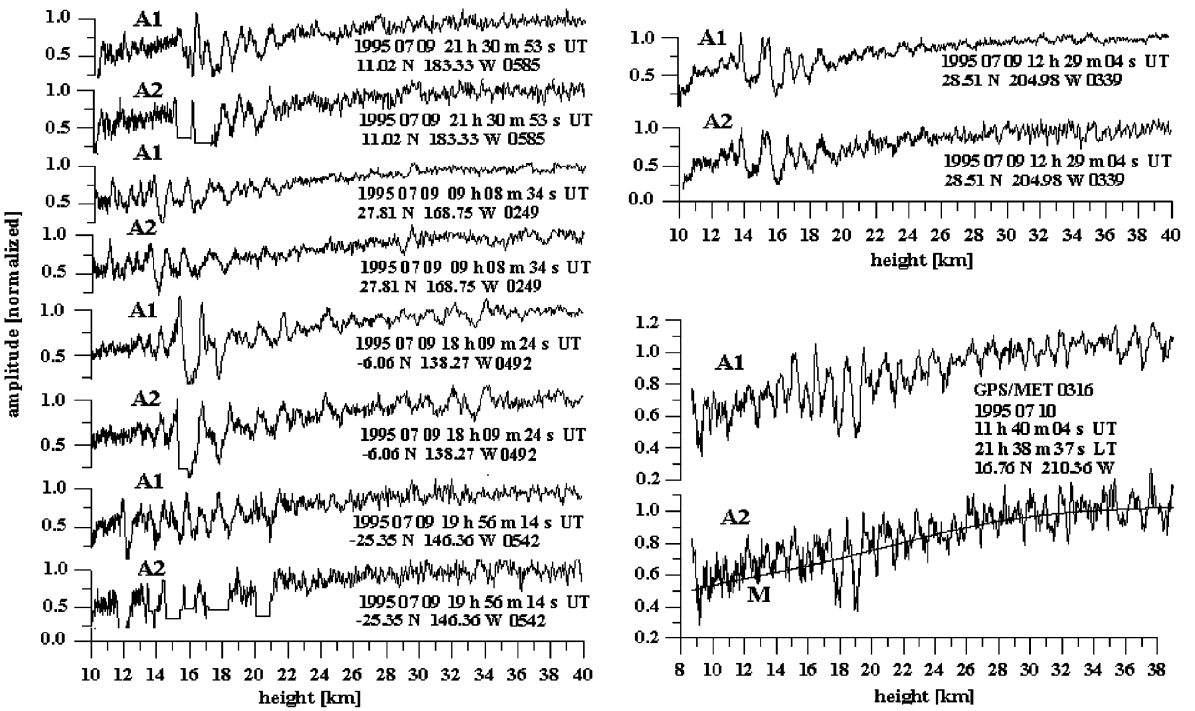

Fig. 2. Height dependence of the amplitudes $A1$, $A2$ for the RO events 0249, 0289, 0316, 0339, 0492, 0542, and 0585 (July 09 and 10, 1995). Wave signatures are especially strong at the heights of 9–20 km and seen simultaneously at both amplitudes (curves A1, A2). Curve M in the right panel indicates result of simulation of the refraction attenuation in the RO region.

information can be obtained on the quantitative characteristics of the wave processes: vertical distribution of the horizontal wind perturbations and its gradient. It is convenient to present the solution of the inverse problem in the simplified approximated form (Liou et al., 2002; Pavelyev et al., 2002)

$$p(t) - p(t_0) = \int_{t_0}^{t} \mathrm{d}tX[t(p_s)\mathrm{d}p_s/\mathrm{d}t, \tag{2}$$

where X is the power attenuation relative to free space owing to the refraction effect for experimental data, p, p_s are the impact parameters relevant to ray GTL and GDL. Eq. (2) allows one to find the temporal dependence of the impact parameter $p(t)$ from the amplitude data if an initial condition is given. The power attenuation $X(t)$ is connected with the derivative $\mathrm{d}\xi/\mathrm{d}p$, where $\xi(p)$ is the refraction angle

$$\mathrm{d}\xi/\mathrm{d}p = [1 - 1/X(t)]B(p); B(p) = (R_1^2 - p^2)^{-1/2} + (R_2^2 - p^2)^{-1/2}. \tag{3}$$

Thus the amplitude data may be used for the restoration of the impact parameter $p(t)$, the refraction angle $\xi(t)$ (Eq. (2)), and the derivative $\mathrm{d}\xi/\mathrm{d}p(t)$, and then for finding the vertical distributions of the refractivity gradient $\mathrm{d}N/\mathrm{d}h$:

$$J(p) = 1/\pi \int_p^{\infty} \mathrm{d}\xi_x'(x)(x^2 - p^2)^{1/2};\ \ \mathrm{d}N/\mathrm{d}H = -n^2(h)J(p)/\{p[1 + J(p)]\} \tag{4}$$

The amplitude information may be used for retrieving the vertical gradient of the temperature. As shown by Pavelyev et al. (2002) for the case of the wet atmosphere a connection exists between the vertical temperature and refractivity gradients

$$[\mathrm{d}T_w(h)/\mathrm{d}h]/T_w(h) = -[N(h)]^{-1}\mathrm{d}N(h)/\mathrm{d}h - \mathrm{T}_x/\mathrm{T}_a, (\mathrm{h}) \tag{5}$$

$$T_w(h) = T(h)/\{1 + 4810\mathrm{e}(h)/[P(h)T(h)]\}, T_x \approx 34.16\,\mathrm{K}/km, \quad T_a(h) = T(h)[1 + 0.378\mathrm{e}(h)/P(h)], \tag{6}$$

where $T(h)$ is the temperature of the atmosphere expressed in Kelvin's degrees, $\mathrm{P}(h)$ and $e(h)$ are the atmospheric and water vapor pressure expressed in hectopascals, respectively. Eqs. (5) and (6) connect the vertical gradient of the refractivity $\mathrm{d}N/\mathrm{d}h$ and the vertical gradient of the "wet" temperature $\mathrm{d}T_w(h)/\mathrm{d}h$. At the height above 10 km Eqs. (5) and (6) can be used for finding the vertical gradient of temperature if the refractivity gradient is known.

Examples of temperature retrieving are shown in Figs. 3 and 4 (panel (a)) for the GPS/MET RO events 0316 and 0339 (July 09, 1995). Dotted curves TB in Fig. 3 and 4 (panel (a)) indicate the background temperature profiles in the RO regions. Dashed curves TU describe dependence $T(h)$ restored from the GPS/MET phase data using the University Consortium for Atmospheric Research (UCAR) technology given in the Internet site http://www.cosmic.ucar.edu/gpsmet/feedback.html. Curves TV demonstrate the average temperature vertical profiles, $TV = (T1 + T2)/2$, where $T1$, $T2$ are

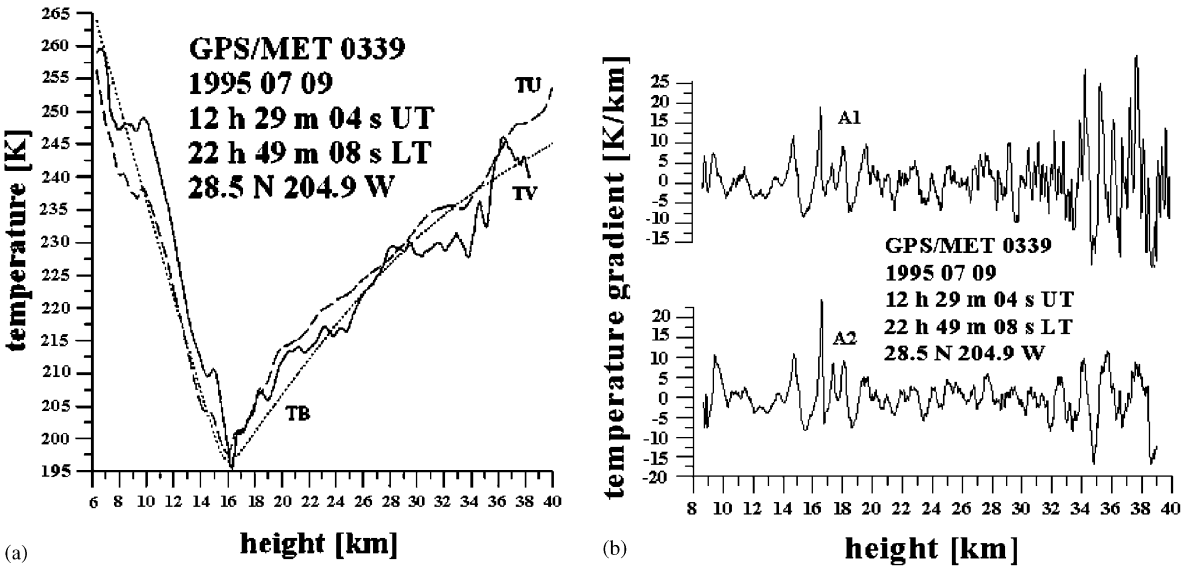

Fig. 3. The temperature and its vertical gradient retrieved on the RO amplitude data for RO event 0339. Panel (a): Curve TV indicates the average of the two retrieved temperature $TV = (T1 + T2)/2$, where $T1$ and $T2$ correspond to the amplitude $A1$ and $A2$, respectively. Dashed curve TU demonstrates the temperature profile calculated from phase data (UCAR retrieval). Dotted curve TB describes the background temperature profile. Panel (b): perturbations of the temperature vertical gradient obtained from the amplitudes $A1$, $A2$.

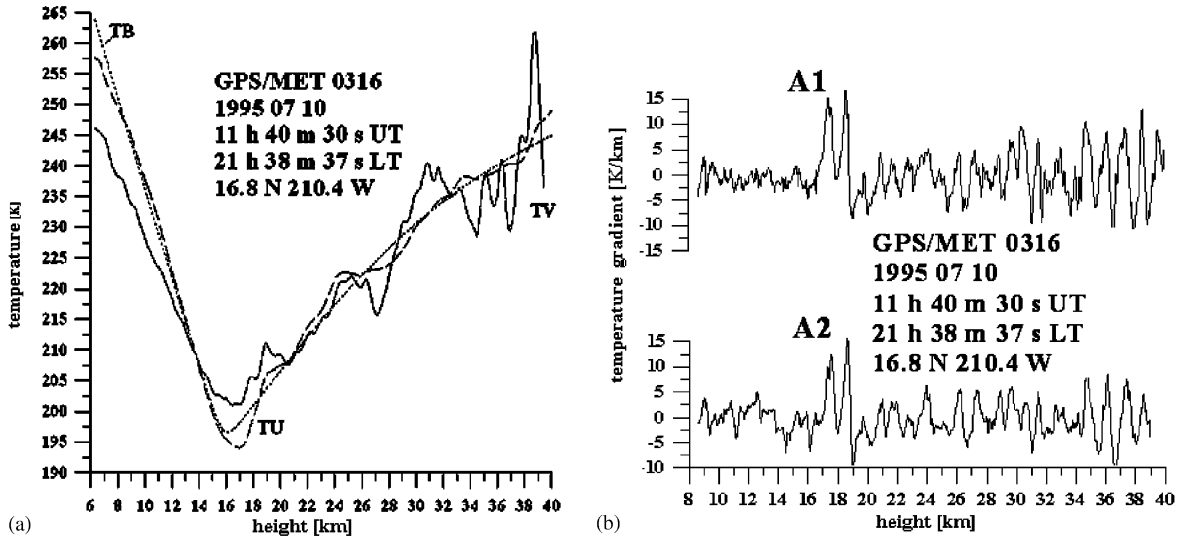

Fig. 4. The same as in Fig. 3 for RO event 0316.

temperatures retrieved from the amplitudes $A1$, $A2$, respectively. Temperature fluctuations are evident in the retrieved temperatures profiles in Figs. 3 and 4 panel (a). Low-frequency variations can correspond to the deflections of the background temperature profile from the approximated values. Fluctuations with spatial periods below 2–4 km can be associated with the GW propagation (Tsuda and Hocke, 2002). The top and bottom curves $A1$, $A2$ in Fig. 3 and 4, panel (b) show the vertical gradients of the temperature corresponding to the high-spatial frequencies in the temperature profiles obtained from the amplitudes $A1$, $A2$. The short spatial periods are clearly seen in the vertical gradient of the temperature shown in Fig. 3 and 4, panel (b). Variations of the temperature gradient are high (about ± 6 K/km) in the tropopause region. It is clearly seen in this region the wave activity with spatial periods 1–2 km. In the stratosphere the high-frequency variations, which can be associated with the GWs, have moderate intensity. However, the wave activity really exists in the height interval 20–40 km as follows from comparison of the curves $A1$, $A2$ in Fig. 3 and 4, panel (b). Vertical distribution of the temperature and its gradient can be used to find the quantitative parameters of the wave structures associated with the GWs. To achieve this aim one can use the polarization and dispersion relationship for GW developed earlier.

3. Horizontal wind perturbations connected with GW influence

We will use the polarization and dispersion relationships, which are valid for the medium-frequency case, when the intrinsic frequency of the GW is many times over the inertial frequency f, but is well below the buoyancy frequency ω_b. The dispersion relation has the form (Eckermann et al., 1995; Fritts and Alexander, 2003)

$$\lambda_h = 2\pi|c - U\ \cos\ \varphi|\omega_b, \tag{7}$$

where λ_h is the vertical wavelength of the GW, U is the background wind speed, c is the ground-based GW horizontal phase speed, and φ is the azimuth angle between the background wind and the GW propagation vectors. Eq. (7) connects the vertical wavelength λ_h with the intrinsic phase speed of the GW $v_i = |c - U\cos\varphi|$, which can be measured by an observer moving with the background wind velocity (Eckermann et al., 1995). The polarization relation connects the complex amplitude of the temperature variations, $t(h)$, with the horizontal wind perturbations v(h), corresponding to the GW influence (Lindzen, 1981):

$$v(h) = Re[ig/(T_b\omega_b)t(h)], \omega_b^2 = g/T_b\Gamma,$$
$$\Gamma = \partial T_b/\partial h + 9.8\,\mathrm{K}/km, \tag{8}$$

where g is the gravity acceleration, Γ is the adiabatic lapse rate, and T_b is the background temperature. Pfister et al. (1993) applied successfully the polarization relation (8) to the case study of the regular GW associated with tropical cyclone. Eckermann et al. (1995), used it for statistical analysis of the rocketsonde data. Tsuda et al. (2000) applied relation (8) to determine a global distribution of the GW potential energy using the RO data. One obtains by differentiating (8)

$$\mathrm{d}v(h)/d\mathrm{h} = \mathrm{d}Re[ig/(T_b\omega_b)t(h)]/\mathrm{d}h$$
$$\approx Re[ig/(T_b\omega_b)\mathrm{d}t(h)/\mathrm{d}h]. \tag{9}$$

Eq. (9) is valid assuming that $T_b(h)$ and $\omega_b(h)$ are slowly changing at the vertical scales $\sim\lambda_h$. The functions T_b and ω_b are known from the model of the atmosphere used for the simulation of the refraction attenuation in the RO region (Fig. 2, curve M in the right panel). To find the function $dv(h)/dh$ from the approximation Eq. (9) one can implement the radio holographic analysis by applying the Hilbert transform (Rabiner and Gold, 1978). We suggest that the amplitude variation is a real part of an analytical function. Under this assumption the temperature vertical gradient and the horizontal wind perturbations are also the real parts of the analytical functions, which are connected with the amplitude variations by inversion formulas and polarization relationship (Liou et al., 2003). The Hilbert transform is a mathematical tool to find the imaginary part of an analytical function using its real part. Practical implementation of the Hilbert transform gives the analytic presentation of the real signal $dt(h)/dh$

$$dt(h)/dh = Re\{a_t(h)\exp[i\Phi_t(h)]\}, \quad (10)$$

where $a_t(h)$ and $\Phi_t(h)$ (real functions) are the amplitude and phase of the vertical gradient of the temperature. The function $dv(h)/dh$ can be restored from (9) using the Hilbert transform. The horizontal wind perturbations $v(h)$ can be found using known dependence $dv(h)/dh$ by integration. The results of restoration are shown in Figs. 5 and 6 panels (a) and (b). The quasi-regular modulation of dv/dh is clearly seen in the experimental data (curves $A1$, $A2$ in Figs. 5 and 6, panel (a)). It is important that the vertical period of this modulation is practically the same as seen in the amplitude variations in Fig. 2, right panel. Thus the process of inversion of the amplitude data does not essentially change the form of the initial spectrum of the amplitude variations. One can directly obtain, without inversion, the approximations of the phase and amplitude parts of the function $dv(h)/dh$ using the Hilbert transform of the variations in the amplitude of the RO signals normalized to the standard altitude dependence of the amplitude (shown by curve M in Fig. 2). However, the amplitude part of $dv(h)/dh$ will be described in this case only by a qualitative manner because of the absence of important scaling factor depending on height. Integration of the wind speed gradient dv/dh (Fig. 5, curves $A1$, $A2$, panel (a)) on height gives the horizontal wind perturbations $v(h)$ (Fig. 5, curves $A1$, $A2$, panel (b), GPS/MET RO event 0339) associated with the GW influence. Some correspondence between the horizontal wind perturbations obtained using amplitude data at frequencies $F1$ and $F2$ is seen in the height interval 8–30 km (Fig. 5, panel (b)). The amplitude of the horizontal wind perturbation is about $\pm$4–6 m/s. Some distinction between the curves $A1$, $A2$ (Fig. 5, panel (b)) in the height interval 30–40 km may be connected with influence of systematic errors caused by possible instabilities of the receiver gain or ionospheric interference. To exclude the possible influence of the systematic errors it is necessary to compare the results of the restoration of the horizontal wind perturbation with aero-logical data. Integration of the average wind speed gradients $dv/dh = [dv_{A1}(h)/dh + dv_{A2}(h)/dh]/2$ (Fig. 6, panel (a)) on height gives the horizontal wind perturbations $v(h)$ relevant to GPS/MET RO event 0316 (Fig. 6, panel (b)). The black curve A corresponds to the experimental data; and the curves 1–4 indicate the RS data relating to two stations in Taiwan: Hualien (1, 3) (24.0°N, 238.4°W) and Taipei (2, 4) (25.0°N, 238.5°W) obtained on July 15, 1995, at 00 h UT and 12 h UT, respectively. The difference between the Taiwan stations and the RO region latitudes and longitudes is $\sim 8^\circ$ and

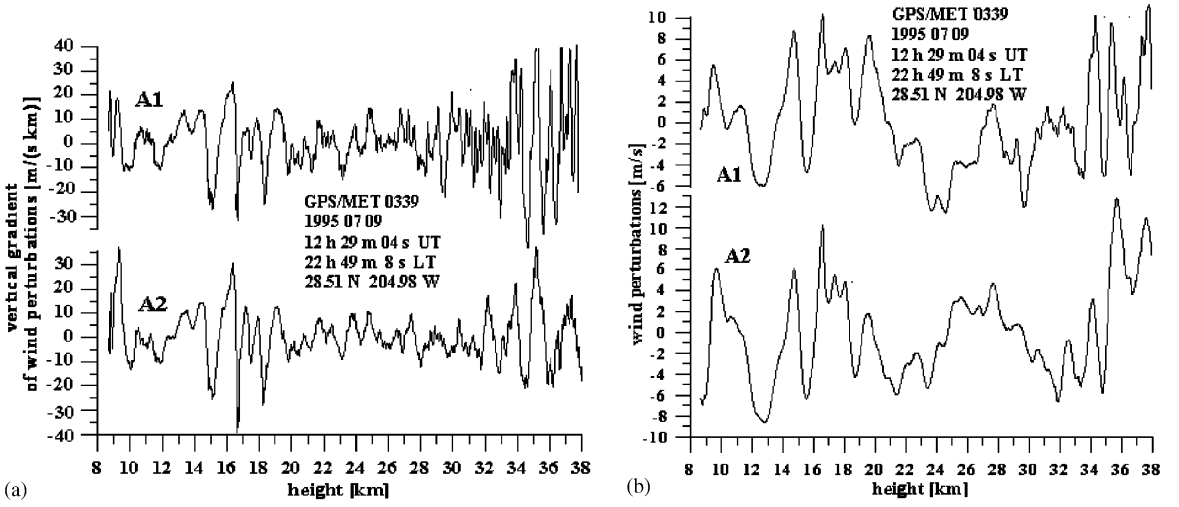

Fig. 5. Results of restoration of the vertical gradient dv/dh (panel a)) and the horizontal wind perturbations $v(h)$ (panel (b)) for GPS/MET RO event 0339.

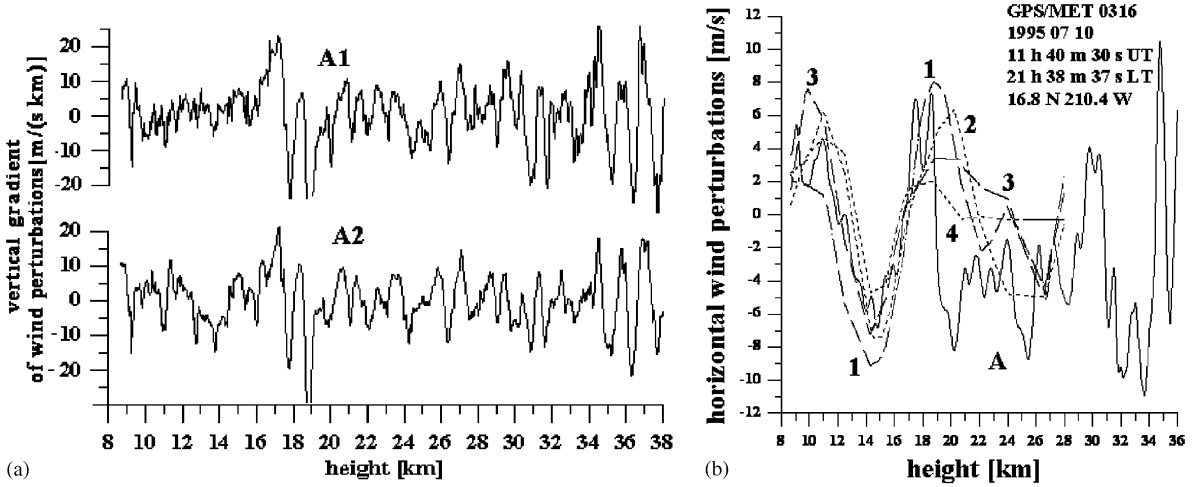

Fig. 6. Results of restoration of the vertical gradient dv/dh (panel (a)) and the horizontal wind perturbations $v(h)$ (panel b)) for GPS/MET RO event 0316. Curve A in panel b) corresponds to the experimental data; the curves 1, 3 (dashed) and curves 2, 4 (dotted) indicate the radiosondes (RS) data relating to two meteorological stations in Taiwan.

$\sim 28^{\circ}$, respectively. The time difference between the RO and RS observations has been chosen in accordance with the average RS background westward wind velocity ~ 10 m/s in the height interval 8–30 km. The RS wind perturbations (curves 1–4) have been obtained by subtracting the polynomial approximation of the fifth power from the experimental vertical profiles of the horizontal wind speed. As follows from Fig. 6 (panel b)) the RS data (1–4) are in fairly good agreement with the experimental results (curve A). The RO values of $v(h)$ (curve A) are variable from ± 1 to ± 9 m/s at the height interval 10–35 km. Some discrepancy ~ 2–4 m/s with RS data exists in the height interval 20–30 km. The difference may correspond to a current state of inversion accuracy. Note, that RS data do not reveal high-spatial frequencies observed in the RO results. As appears, this is due to smoothing effects of the RS measurements. Note also, that difference between the RS and experimental data may be connected with the instability of the receiver gain and the transmitter power, and increasing low-frequency noise (which contain trends and bias) owing to integration during the inversion process.

4. 1-D Image of the GW activity and intrinsic phase speed of GW in the atmosphere

After applying the Hilbert transform one can obtain from Eqs. (9) and (10) the amplitude and phase $a(h)$, $\Phi(h)$ associated with the vertical gradient of the horizontal wind speed variations: $dv(h)/dh = [dv_{A1}(h)/dh + dv_{A2}(h)/dh]/2 = a(h)\cos\Phi(h)$, where $a(h)$ and $\Phi(h)$ are the amplitude and phase of the analytic signal relevant to $dv(h)/dh$. Note, that summation of data of two independent amplitude channels $A1$, $A2$ can diminish the statistical and independent systematic errors in the experimental data The functions $a(h)$, $\Phi(h)$ present together a 1-D "radio image" of GW.

The height dependence of the GW amplitude $a(h)$ and phase $\Phi(h)$ are shown in Fig. 7, left and right panel, respectively, by curves 1–6. The phase curves 1-6 of the 1-D GW radio image have different dependence on the height for considered RO events. The phase curve 2–4 relevant to the GPS/MET events 0339, 0542, and 0585 indicate increasing spatial frequency of the GW with height in opposition to curves 1, 5, and 6, which demonstrate decreasing of the spatial frequency for GPS/MET events 0316, 0249, and 0492. The phase in the GPS/MET event 0492 (curve 6 in Fig. 7, right panel) changes linearly, in average, as a function of the height h, thus corresponding to nearly monochromatic GW. The amplitude, relevant to the GPS/MET RO event 0492 (curve 6 in Fig. 7, left panel), demonstrates essential changes in the interval 0.5–25 m s^{-1} km^{-1}) in the tropopause region at height 15–17 km. For this event one can see in Fig. 7, left panel, altitudes with high (17–19, 21–23, 24–25, and 32–35 km) and low (20–21, and 26–31 km) GW activity. The position of relatively high GW amplitude in the interval 32–35 km is coinciding with the GW breaking zone disposed at height interval 34–37 km observed earlier in the Andes area by Eckermann and Preusse (1999). For the GPS/MET RO event 0524 (curve 3 in Fig. 7, left panel) the amplitude changes are concentrated mainly below 22 km. It follows from Fig. 7 that the GW "radio images" contain important information on the height distribution of the GW activity in the RO regions. The detailed information on the height distribution of the

spatial frequency of the GW can be obtained by differentiating the phase $\Phi(h)$ (curves 1–6 in Fig. 7, right panel). After differentiating one can obtain the spatial frequency f and the vertical wavelength $\lambda_h = 2\pi/f$ as functions of height and then estimate the intrinsic phase speed of the GW v_i using relation (7). As seen in Fig. 8 (curves 1–6) the value f changes in the range of 1–15 rad/km.

Corresponding values of the intrinsic phase speed are changing in the interval 2-20 m/s. High variability of the intrinsic phase speed can be observed for event 0585 and 0249 (curve 4 and 5 in Fig. 8, right panel). Low variability of the intrinsic phase speed is seen for GPS/MET RO events 0316 and 0339 (curves 1 and 2 in Fig. 8, right panel). The values of the intrinsic phase speed in the interval 2–10 m/s are similar to the intrinsic phase

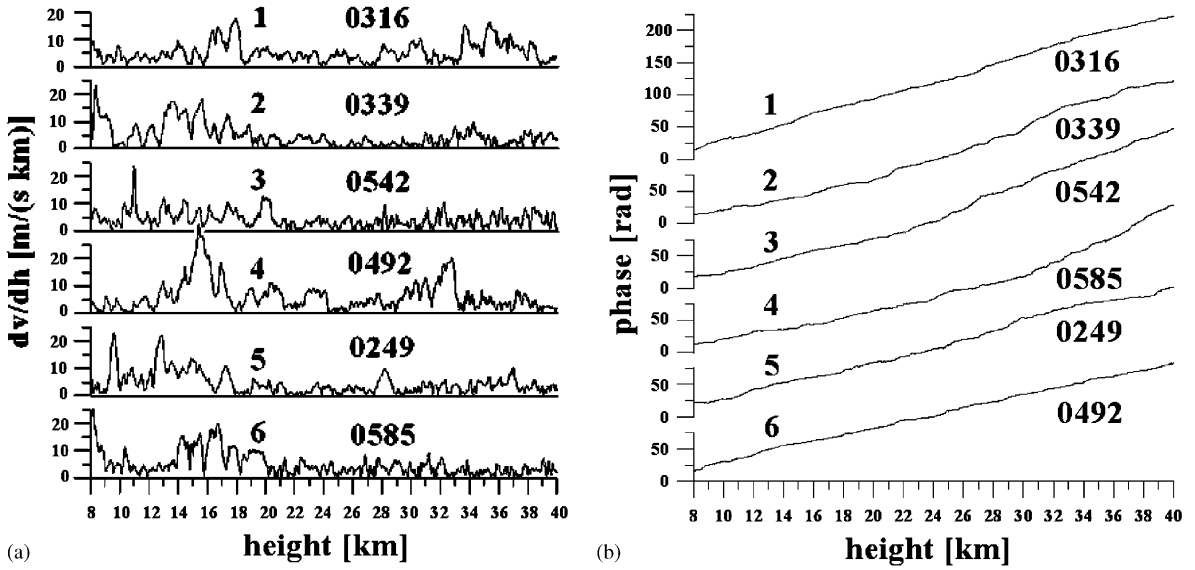

Fig. 7. 1-D radio images of GW for GPS/MET RO events 0316, 0339, 0542, 0585, 0249, and 0492 (curves 1–6). Left panel: amplitude of GW as function of height. Right panel: the altitude phase dependence of GW.

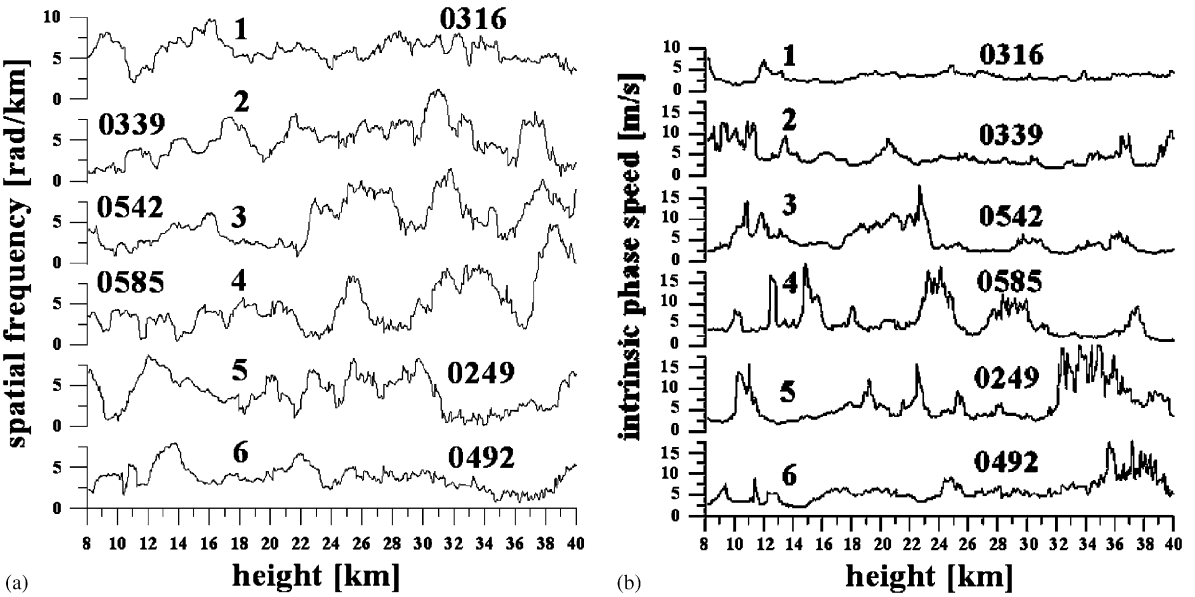

Fig. 8. Spatial frequency (left panel) and intrinsic phase speed (right panel) of GW for GPS/MET RO events 0316, 0339, 0542, 0585, 0249, and 0492 (curves 1–6).

speed measured by rocketsondes (Eckermann et al., 1995) and satellite (Eckermann and Preusse, 1999) and may correspond to the quiet conditions in the atmosphere. Thus the 1-D "radio image" of GW is useful tool for description of the GW activity and its intrinsic phase speed as function of height in the atmosphere.

5. Conclusions

Amplitude variations of the RO signal contain important information on the vertical structure of the upper troposphere and lower stratosphere including the vertical profiles of the temperature and its gradient. Application of the amplitude method to the analysis of the RO data gives simultaneously detailed vertical profiles of the temperature and its gradient in the atmosphere in height interval 5–40 km. Sharp variations in the vertical gradients correspond to the tropopause region at the heights 10–17.5 km where gradients changed in the range from -9 K/km to 6 K/km. Variations of the vertical gradient in the stratosphere revealed wave-like structures (clusters) with vertical periods of about 0.8–2 km. These structures can be associated with the quasi-periodical GW propagating through the tropopause to stratosphere. The vertical period of the GW is ~0.8–4 km. Accuracy of the restoration increases with diminishing of the periods of the vertical gradients of the refractivity and temperature. The amplitudes of the RO signals at both GPS frequencies are sensitive to the wave structures in the upper troposphere and stratosphere. The amplitude wave trains in the RO data can be used for retrieving the phase and amplitude of the wave structures in the atmosphere as functions of height. This property of the amplitude of the satellite signals is important for direct measurements of the regular distribution of the GW activity in the height interval 8–40 km on a global scale. For analysis of the amplitude variations a new analytical method is introduced. The method uses the polarization and dispersion relations and Hilbert transform to restore 1-D image of the GW (the amplitude and phase of the GW as functions of height). The analytic form of the GW presentation is convenient for the analysis of the experimental data and can be implemented for the determination of the GW intrinsic phase speed and the horizontal wind perturbations associated with the GW influence. For validation of the new retrieval method, we compare the wind speed perturbations retrieved from the GPS/MET data to the corresponding wind measurements obtained in situ by nearby balloon RS. The RS measurements agree well with the analyzed GPS observations. The discrepancy is about 1–2 m/s for the heights below 18 km and 2–4 m/s for the heights of 20–30 km. The vertical gradients of the horizontal wind speed changed more essentially from ± 0.5 up to $\pm 20\,\mathrm{m\,s^{-1}\,km^{-1}}$. The RO method appears to have a considerable promise to measure the regular characteristics of the GW and the consequent vertical distribution of the horizontal wind perturbations.

Acknowledegments

We are grateful to UCAR for access to the GPS/MET data. We express our gratitude to Prof. A. Koustov (Saskatoon, Canada) and Prof. V. Vorob'ev (Moscow, Russia) for detailed discussions, which help us to improve our paper. We are grateful to National Science Council of Taiwan, ROC, for financial support under the Grants NSC 92-2811-M008-001, NSC 91-2111-M008-029, and Office of Naval Research (ONR) of USA under Grant N00014-00-0528. Work has been partly supported by Russian Fund of Basic Research, Grant No. 03-02-17414.

References

Anthes, R.A., Rocken, C., Kuo, Y.-H., 2000. Applications of COSMIC to meteorology and climate. Terrestrial, Atmospheric and Oceanic Science 11, 115–156.

Eckermann, S.D., Preusse, P., 1999. Global measurements of stratospheric mountain waves from space. Science 286, 1534–1537.

Eckermann, S.D., Hirota, I., Hocking, W.A., 1995. Gravity wave and equatorial wave morphology of the stratosphere derived from long-term rocket soundings. Quarterly Journal of Royal Meteorological Society 121, 149–186.

Feng, D.D., Herman, B.M., 1999. Remotely sensing the Earth's atmosphere using the Global Positioning System (GPS)—the GPS/MET data analysis. Journal of Atmospheric and Ocean Technology 16, 990–1002.

Fritts, D.C., Alexander, M.J., 2003. Gravity wave dynamics and effects in the middle atmosphere. Reviews of Geophysics 41, 1–64.

Hajj, A., Kursinski, E.R., Romans, L.J., Bertiger, W.I., Leroy, S.S., 2002. A technical description of atmospheric sounding by GPS occultation. Journal of Atmospheric and Solar-Terrestrial Physics 64, 451–469.

Igarashi, K., Pavelyev, A., Hocke, K., Pavelyev, D., Kucherjavenkov, I.A., Matugov, S., Zakharov, A., Yakovlev, O., 2000. Radio holographic principle for observing natural processes in the atmosphere and retrieving meteorological parameters from RO data. Earth Planets Space 52 (11), 868–875.

Igarashi, K., Pavelyev, A., Hocke, K., Pavelyev, D., Wickert, J., 2001. Observation of wave structures in the upper atmosphere by means of radio holographic analysis of the RO data. Advances in Space Research 27 (6–7), 1321–1327.

Kalashnikov, I., Matugov, S., Pavelyev, A., Yakovlev, O., 1986. Analysis of the features of radio occultation method for the Earth's atmosphere study. In: Electromagnetic Waves in the Atmosphere and Space. Nauka, Moscow, pp. 208–218 (in Russian).

Lindzen, R.S., 1981. Turbulence and stress owing to gravity wave and tidal breakdown. Journal of Geophysical Research 86 (C10), 9707–9714.

Liou, Y.-A., Pavelyev, A.G., Huang, C.-Y., Igarashi, K., Hocke, K., 2002. Simultaneous observation of the vertical gradients of refractivity in the atmosphere and electron density in the lower ionosphere by RO amplitude method. Geophysical Research Letters 29 (19) 43-1–43-4.

Liou, Y.A., Pavelyev, A.G., Huang, C.Y., Igarashi, K., Hocke, K., Yan, S.K., 2003. Analytic method for observation of the gravity waves using radio occultation data. Geophysical Research Letters 30 (20), ASC 1-1–1-5.

Nagpal, O.P., 1979. The sources of atmospheric GW. Contemporary Physics 20, 593–609.

Nastrom, G.D., Van Zandt, T.E., Warnock, J.M., 1997. Vertical wave number spectra of wind and temperature from high-resolution balloon soundings over Illinois. Journal of Geophysical Research 102 (D6), 6685–6701.

Nastrom, G.D., Hansen, A.R., Tsuda, T., Nishida, M., Ware, R., 2000. A comparison of gravity wave energy observed by VHF radar and GPS/MET over central North America. Journal of Geophysical Research 105 (D4), 4685–4687.

Pavelyev, A., Igarashi, K., Reigber, C., Hocke, K., Wickert, J., Beyerle, G., Matyugov, S., Kucherjavenkov, A., Pavelyev, D., Yakovlev, O., 2002. First application of radioholographic method to wave observations in the upper atmosphere. Radio Science 37 (3) 15-1–15-11.

Pfister, L., Chan, K.R., Bui, T.P., Bowen, S., Legg, M., Gary, B., Kelly, K., Proffit, M., Starr, W., 1993. Gravity waves generated by a tropical cyclone during the STEP tropical field program: a case study. Journal of Geophysical Research 98 (D5), 8611–8638.

Preusse, J.M., Smolarkiewicz, S., Garcia, R.R., 1996. Propagation and breaking at high altitudes of GW excited by tropospheric forcing. Journal of Atmospheric Sciences 53, 2186–2216.

Rabiner, L., Gold, B., 1978. Theory and Application of Digital Signal Processing. Prentis Hall, Englewood cliffs, NJ 551pp.

Reigber, Ch., Lühr, H., Schwintzer, P., 2002. CHAMP mission status. Advances in Space Research 30 (2), 129–134.

Sica, R.J., Russell, A.T., 1999. Measurements of the effects of gw in the middle atmosphere using parametric model of density fluctuations. Part I: vertical wavenumber and temporal spectra. Journal of Atmospheric Science 56, 1308–1329.

Sokolovskiy, S.V., 2000. Inversion of RO amplitude data. Radio Science 35 (7), 97–105.

Steiner, A.K., Kirchengast, G., 2000. Gravity wave spectra from GPS/MET occultation observations. Journal of Atmospheric and Oceanic Technology 17, 495–503.

Tsuda, T., Hocke, K., 2002. Vertical wave number spectrum of temperature fluctuations in the stratosphere using GPS occultation data. Journal of the Meteorological Society of Japan 80 (4B), 228–241.

Tsuda, T., Nishida, M., Rocken, C., Ware, R.H., 2000. A global morphology of gravity wave activity in the stratosphere revealed by the GPS occultation data (GPS/MET). Journal of Geophysical Research 105 (D6), 7257–7273.

Vorob'ev, V.V., Gurvich, A.S., Kan, V., Sokolovskiy, S.V., Fedorova, O.V., Shmakov, A.V., 1999. Structure of the ionosphere from the radio-occultation GPS-"Microlab-1" satellite data: preliminary results. Earth Observations and Remote Sensing 15, 609–622.

Ware, R., Exner, M., Feng, D., Gorbunov, M., Hardy, K., Herman, B., Kuo, Y.-H., Meehan, T., Melbourn, W., Rocken, C., Schreiner, W., Sokolovskiy, S., Solheim, F., Zou, X., Anthes, R., Businger, S., Trenberth, K., 1996. GPS soundings of the atmosphere from low earth orbit: preliminary results. Bulletin of the American Meteorological Society 77, 19–40.

Wickert, J., Reigber, Ch., Beyerle, G., Konig, R., Marquardt, Ch., Schmidt, T., Grunwaldt, L., Galas, R., Meehan, T., Melbourne, W.G., Hocke, K., 2001. Atmosphere sounding by GPS RO: first results from CHAMP. Geophysical Research Letters 28, 3263–3266.